Electronic Supplementary Material (ESI) for Environmental Science: Nano.

Identifying Active Sites of Co_3O_4 Catalysts towards C_2H_2 Oxidation by Combined Computational and Experimental Methods

Jianlin Deng, Meng Gao, Meng Wang, Yaozhao Li, Weiyu Song, Lu Wang, Huiling Zheng, Jian Liu*

1. Calculational methods

Density Function Theory (DFT) studies were performed with the Vienna Ab Initio Simulation Package (VASP) [1, 2], using the spin-polarized approach. The exchange-correlation and the core-valence electron interaction were described by the Perdew-Burke-Erzonhoff (PBE) of the generalized-gradient approximation (GGA) [3] and the projector augmented wave (PAW) method [4], respectively. In all calculations, the electronic energies and force threshold were -0.05 eV/Å and 10^{-4} eV for the optimization and transition-state search, respectively. The cutoff energy was set of 400 eV and a 3 × 2× 1 *k*-point mesh was used for Co_3O_4 surface slabs. It is necessary to consider Coulomb and exchange interactions of Co_3O_4 [5, 6], for its highly correlated electronic states. U = 3 was adopted to provide a better description of the electronic structure and the surface reactivity [7]. The optimized bulk lattice parameter is 8.135 Å, which is close to the experimental value of 8.08 Å and the calculational value of 8.16 Å [8]. The magnetic moment of Co^{2+} ($\mu_{Co}{}^{2+}$) calculated in our work is 2.67 μB, which is in accordance with the reference [7]. The climbing-image nudged elastic band module was employed to locate the transition states [9], the found of which were further verified to be a first-order saddle point by numerical frequency analysis.

The adsorption energy of surface species is calculated by the way that the energy after adsorption minus the sum of energies of the surface and gas before adsorption respective. In general, a negative adsorption energy indicates that the adsorption process is exothermic. The oxygen vacancy formation energy was calculated by subtracting Co_3O_4 surface energy from the total energy of the defective Co_3O_4 surface and half an oxygen molecule.

2. Analytical Methods

X-ray diffraction (XRD) spectrum were acquired on a Bruker D8 Advance powder X-ray diffractometer using CuKα (k = 0.15406 nm) radiation with a Nickel filter. The operating voltage and current is 40 kV and 40 mA, respectively. And the scanning rate in the 2θ range of 10-90° is 4°/min. JCP-DS reference data were used for phase identification of XRD spectra. Brunauer−Emmet−Teller (BET) surface areas were calculated using an SSA6000 instrument. Samples were pretreated at 150 °C for 5 h in vacuum. Quanta 200F field emission Scanning Electron Microscopy (SEM) was used to observe the surface morphology of the catalysts (accelerating

voltages of 5 kV). The SEM samples were sprinkled on conducting resin and coated with 10 nm Au before measurements. The transmission electron microscopy (TEM) and high-resolution TEM (HRTEM) images were observed by using a JEOL JEM-2100 transmission electron microscope. The TEM sample was obtained by dropping the nanoparticles/ethanol mixture onto a carbon-coated copper grid. PHI-1600 ESCA instrument was used to get the X-ray photoelectron spectroscopy (XPS) measurements with Mg, Kα as the excitation source. The O_2-TPD and H_2-TPR was performed using Micromeritics AutoChem 2920 equipment and Quanta-chrome Autosorb-iQ-TPX, respectively. TPO-MS (Hiden QIC-20) analysis was performed to investigated CO_2 generated from the residual carbon and C_2H_2. The TPO is the same as the above. Reactant gases (50 mL/min, balanced with Ar) contain 10% O_2 with and without 150ppm C_2H_2, respectively. The relative intensity of outlet gas CO_2 was analyzed by MS.

3. Microkinetic methods

The microkinetic simulation is performed by MKMCXX software [10]. The reaction rate constant can be calculted by the Eyring equation (3):

$$k = Ae^{-\frac{E_a}{k_bT}} \quad (3)$$

where k is reaction rate constant; E_a is the activation barrier; k_b is Boltzmann constant; A is the prefactor; T is temperature in Kelvin.

The adsorption and desorption rates of non-activated molecular are derived from the Hertz-Knudsen kinetics by equation (4-6) [11]:

$$k_{ads} = S\frac{PA}{\sqrt{2\pi m k_b T}} \quad (4)$$

$$k_{des} = A\frac{k_b T^3}{h^3}\frac{2\pi k_b}{\sigma\theta_{rot}}\exp\left(\frac{-E_{des}}{RT}\right) \quad (5)$$

$$r = k_{ads}\cdot p_A - k_{des}\cdot\left[A_{ads}\right] \quad (6)$$

Here S is the sticking coefficient; P is the partial pressure of adsorbate in the gas; A is the area of the surface site; m is the mass of the molecule, σ is the symmetry number, and θ_{rot} represent the characteristic temperature for rotation, respectively.

For the elementary reaction step, the rate constant of M components is derived by the differential equation (7):

$$r_i = \sum_{j=1}^{N}\left(k_j v_i^{\,j} \prod_{k=1}^{M} c_k^{\,v_k^{\,j}} \right) \tag{7}$$

Where v_i, k_j and c_k are the stoichiometric coefficient of component i in reaction step k, reaction rate constant and the concentration of component k on the surface.

The degree of rate control (X_{RC}), which represents the variance of the overall rate of each steps on slight changes in the energy of transition state, is calculated by equation (8):

$$X_{RC,i} = \frac{k_i}{r}\left(\frac{\partial r}{\partial k_i}\right)_{k_{j\neq i},K_i} = \left(\frac{\partial \ln r}{\partial \ln k_i}\right)_{k_{j\neq i},K_i} \tag{8}$$

Where k_i is the rate constant; K_i stands for the equilibrium constant, and r represents the reaction rate.

4. Results

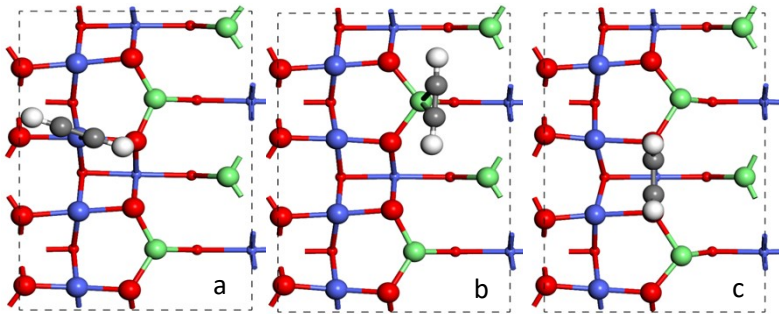

Fig. S1. The adsorption configurations of C_2H_2 on different sites of Co_3O_4 (110)-A surface. Co^{3+} site (a), Co^{2+} site (b), O_{3c} sites (c). The corresponding adsorption energy for a, b and c is -0.42, -0.62 and -2.55eV, respectively.

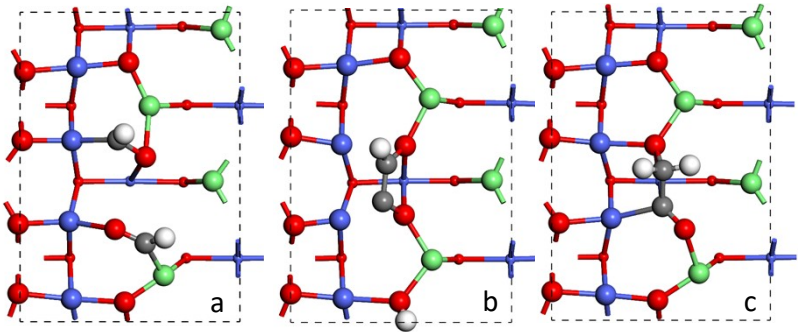

Fig. S2. The configurations formed by the cleavage of C-C and C-H bond of C_2H_2 on Co_3O_4 (110)-A surface. direct C-C cleavage (a), C-H cleavage (H→O_{3c}) (b), C-H cleavage (inner-molecular H shift) (c).

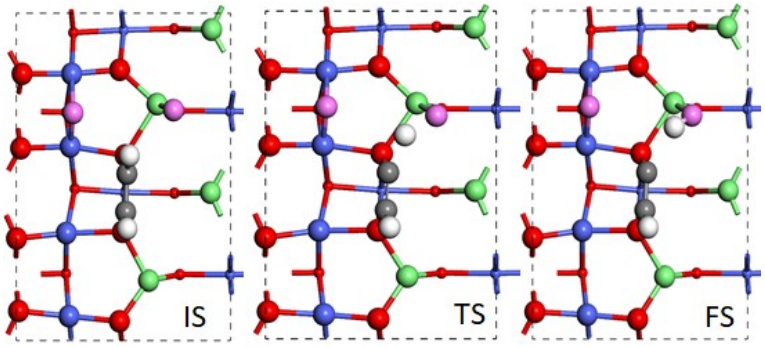

Fig. S3. The dehydrogenation path of CHCH on Co_3O_4 (110)-A surface. IS, TS and FS indicates initial state, transition state and final state, respectively.

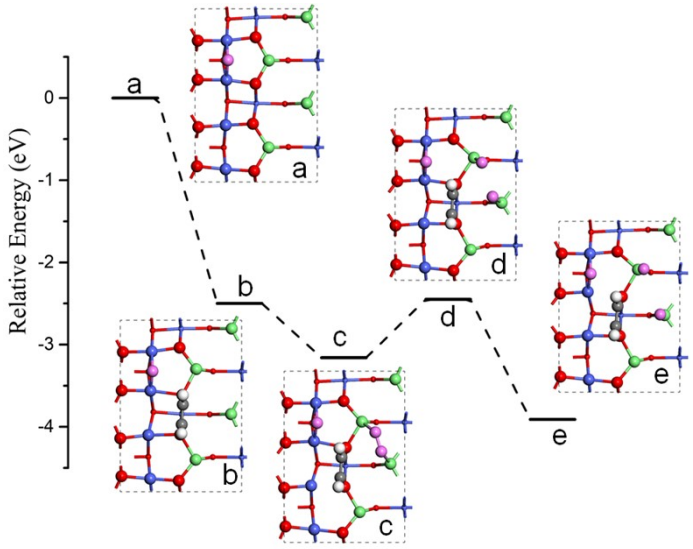

Fig. S4. The reaction path of the residual O in the next reaction cycle. The residual O (a); The adsorption of C_2H_2 (b); the adsorption of O_2 (c); the transition state of O_2 dissociation (d); the dissociation of O_2 (e).

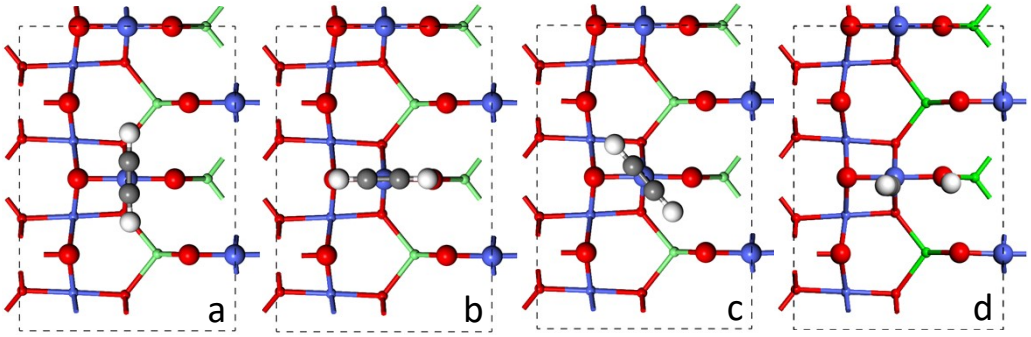

Fig. S5. The adsorption (a, b, c) and dissociation (d) configurations of C_2H_2 on Co_3O_4 (110)-B surface. The calculated adsorption energy for a, b and c is -0.4, -0.33 and -0.46 eV, respectively.

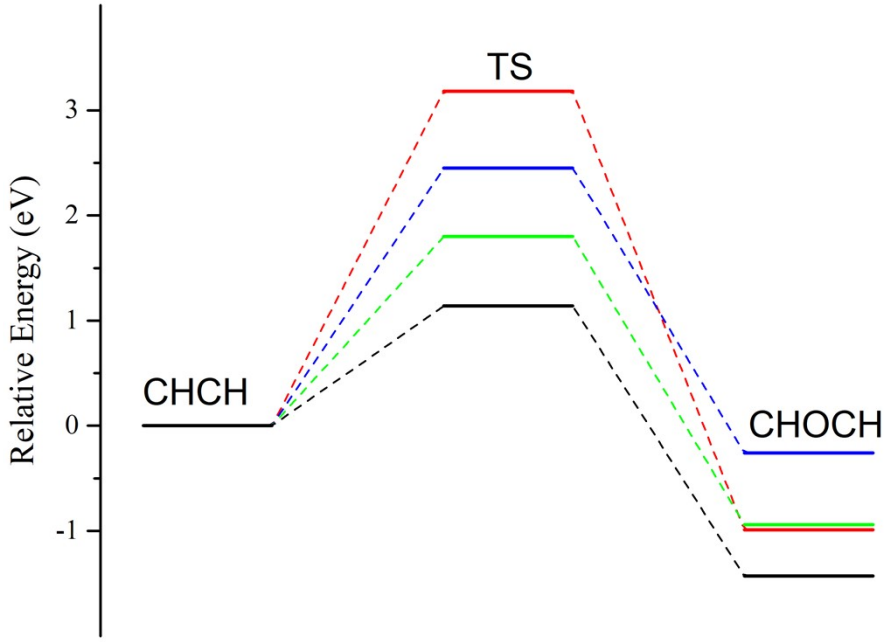

Fig. S6. The energy diagram for CHCH and different O atoms to form CHOCH. Lattice O_{3c} (red), lattice O_{2c} (blue), the adsorption O of the three-membered ring structure (green), the adsorption O of side-on structure (black).

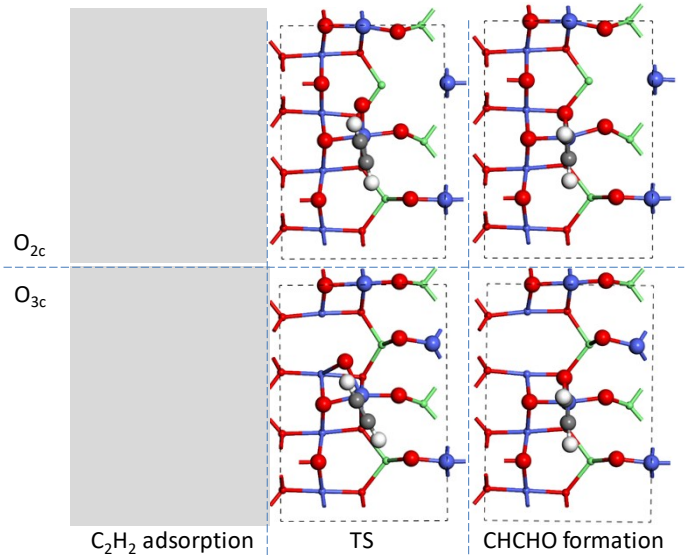

Fig. S7. The reaction process of C_2H_2 with lattice oxygen (O_{2c} and O_{3c}) to form CHCHO on Co_3O_4 (110)-B surface.

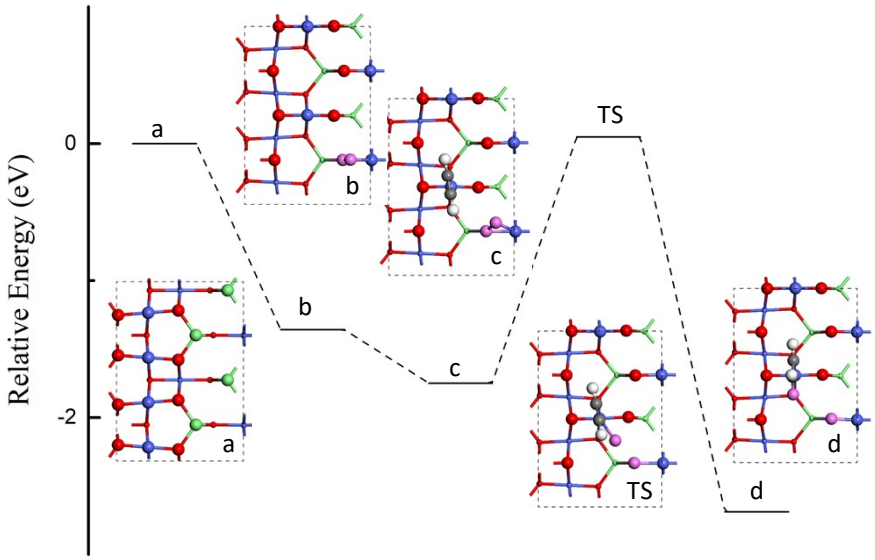

Fig. S8. The reaction process of C_2H_2 with adsorbed oxygen (three-membered ring structure) to form CHCHO on Co_3O_4 (110)-B surface. Co_3O_4 (110)-B surface (a); the adsorption of O_2 (b); the adsorption of C_2H_2 (c); the formation of CHOCH (d).

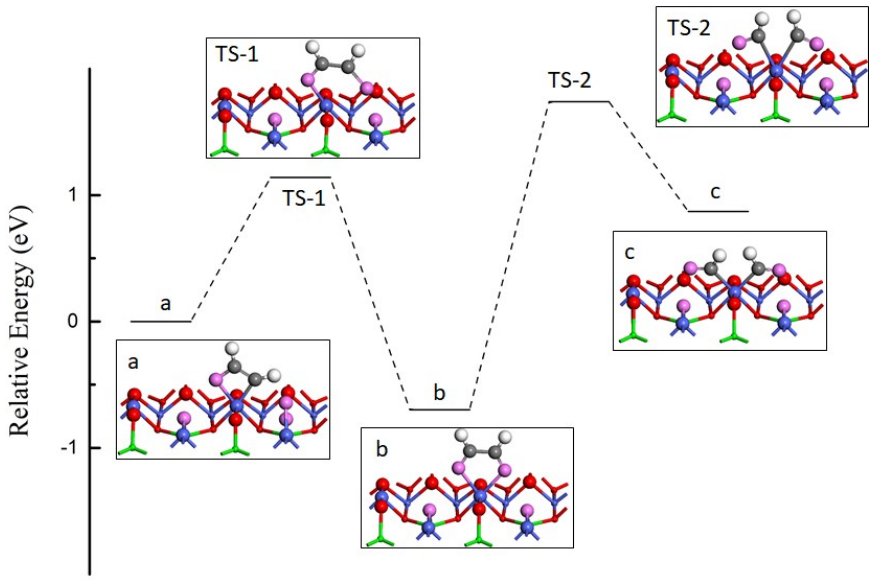

Fig. S9. The reaction path of CHOCH to CHO by forming CHOCHO species on Co_3O_4 (110)-B surface. CHOCH (a), CHOCHO (b), CHO-CHO (c).

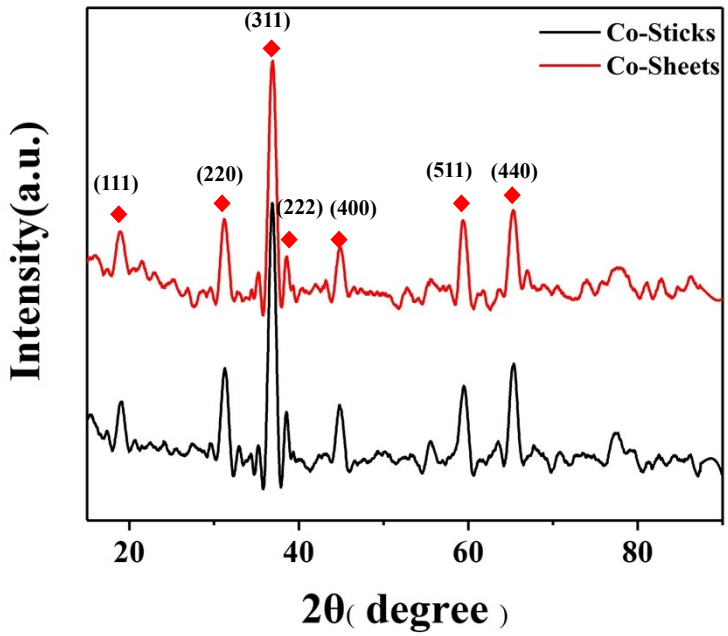

Fig. S10. XRD patterns of Co_3O_4-Sticks and Co_3O_4-Sheets catalysts prepared by hydrothermal synthesis method.

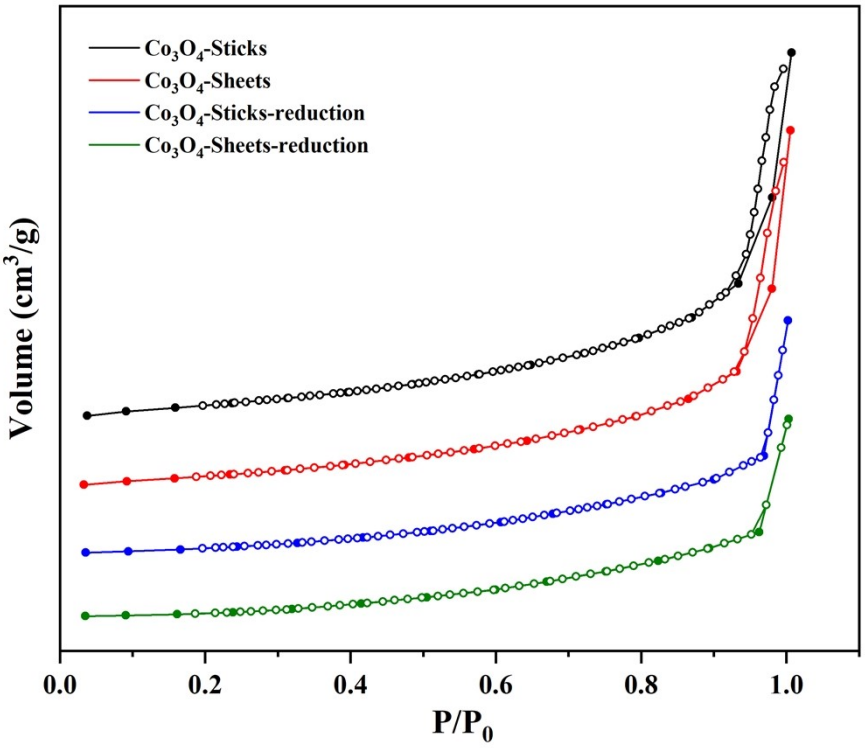

Fig. S11. N_2 adsorption−desorption isotherms of Co_3O_4 catalysts.

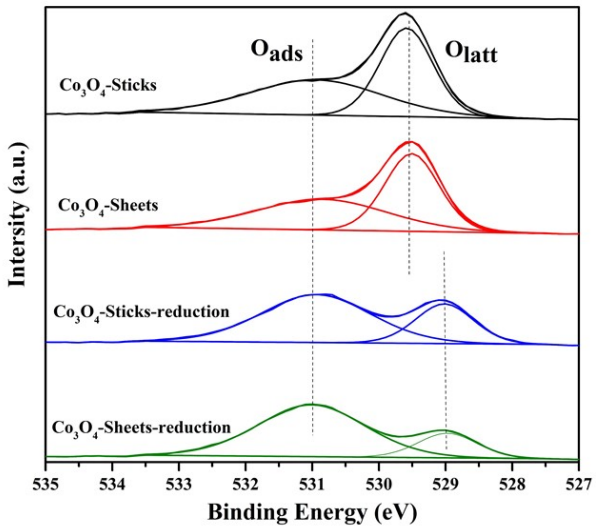

Fig. S12. X-ray photoelectron spectra of O 1s regions for Co_3O_4-Sticks, Co_3O_4-Sheets, Co_3O_4-Sticks-reduction and Co_3O_4-Sheets-reductions catalysts.

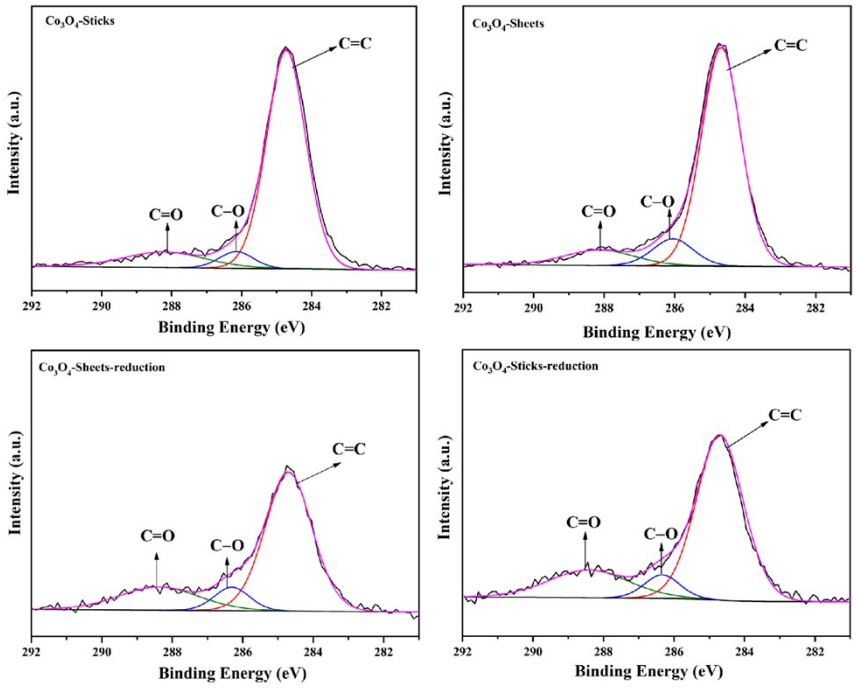

Fig. S13. X-ray photoelectron spectra of C 1s regions for Co_3O_4, Co_3O_4-Sticks, Co_3O_4-Sheets, Co_3O_4-Sticks-reduction and Co_3O_4-Sheets-reductions catalysts.

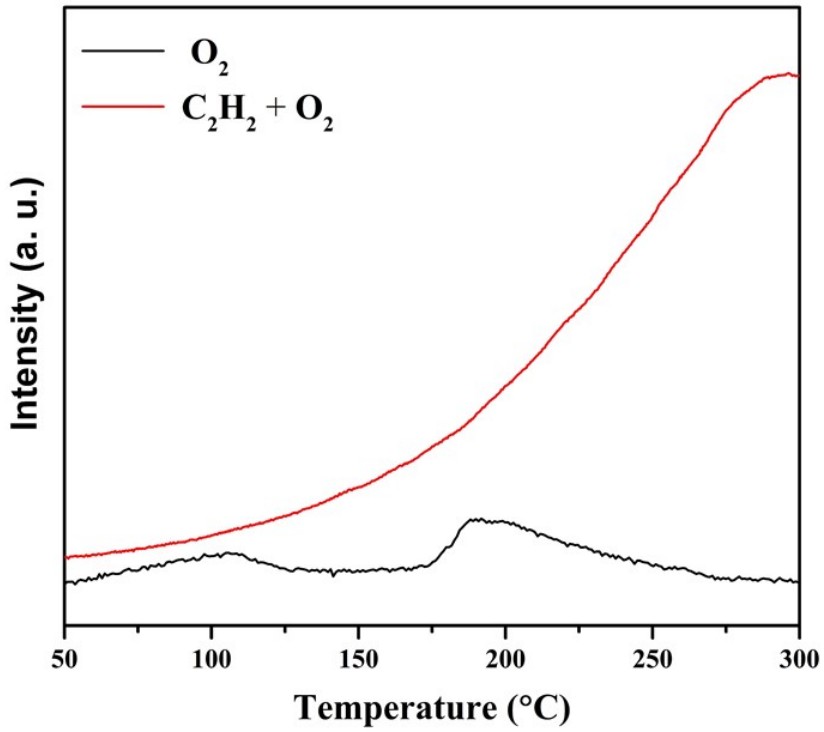

Fig. S14. The relative intensity of CO_2 from TPO-MS.

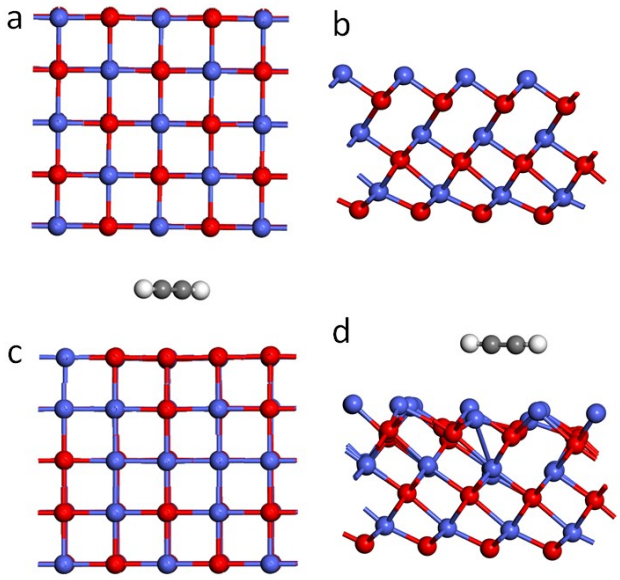

Fig. S15. The configurations of CoO (100) and (111) surface (a, b). The adsorption configurations of C_2H_2 on CoO (100) and (111) surface (c, d).

Bulk CoO crystallizes in the rock salt structure, with both Co and O atoms in octahedral environments. Ground-state CoO exhibits type-II antiferromagnetic (AFM-II) spin ordering, with antiparallel ordering of adjacent (111) planes [12]. The U_{eff} was set as 4.1 eV, giving a lattice constant of 4.26 Å, in very good agreement with the experimental value of 4.262 Å [13]. We considered CoO (100) and (111) structures with AFM on Co ions in alternating planes along (100), and (111) direction, which have the lowest energy [14]. The CoO (100) and (111) surfaces were composed of 5 atomic layers, with a 2 × 2 supercell. The vacuum between slabs was 12 Å, and a 2 × 2× 1 k-point mesh was used. The bottom two layers were fixed, and the top three atomic layers were all relaxed. Co-terminated CoO (111) surface was adopted for its minimum adsorption energy.

Table S1. The temperature and the selectivity to CO_2 of C_2H_2 combustion over as-prepared Co_3O_4 catalysts.

Catalysts	T_{10}/°C	T_{50}/°C	T_{100}/°C	S_{CO2}^{m}/%
Co_3O_4-Sticks	162	230	254	100.0
Co_3O_4-Sheets	107	164	198	100.0
Co_3O_4-Sticks-reduction	149	217	236	100.0
Co_3O_4-Sheets-reduction	104	144	166	100.0

Table S2. Chemical and physical parameter and surface compositions of the different catalysts.

Catalysts	surface area (m^2/g)	particle size (nm)	Co^{2+}/Co^{3+}	O_{ads}/O_{latt}	C concentrations (at. %)
Co_3O_4-Stick	18.2	10.7	0.40	1.09	8.86
Co_3O_4-Sheet	15.7	14.4	1.07	1.07	8.01
Co_3O_4-Stick-reduction	9.8	10.7	0.56	2.21	8.88
Co_3O_4-Sheet-reduction	6.7	14.4	1.64	3.76	8.14

Table S3. The activation energy, forward and backward rate constants of each elementary reaction step of C_2H_2 oxidation on Co_3O_4 (110)-A surface.

Reaction steps	activation energy (kJ/mol)	forward rate constants	backward rate constants	degree of rate control
CHCH + * → CHCH*	0	8.876	2.635e-8	0
O_2 + # → O_2#	0	3.417e4	3.415e4	2.078e-8
O_2# → O-O#	62.5	8.876	3.974e-11	4.541e-5
CHCH* + O-O# → CHCHO* + O#	1.9	8.876	8.092e-9	1.151e-11
CHCHO* + O_2# → CHOCHO* + O#	1.0	8.876	2.249e-22	7.726e-7
CHOCHO* → CHO-CHO*	109.6	8.876	1.700e-3	9.998e0
CHO-CHO* + O# → CO_2-CHO* + OH#	57.7	8.876	3.382e-4	2.000e-4
CO_2-CHO* + O# → CO_2-CO_2* + OH#	57.7	8.876	6.824e-33	3.895e-6
CO_2-CO_2* → 2 CO_2 (g) + O_{vac}*	0	0	8.876	5.129e-14
O_{vac}* + O_2 → *	0	8.876	1.938e-27	2.078e-8
2 OH# → H_2O# + #	50	8.876	2.180e-3	6.099e-7
H_2O# → H_2O(g) + #	0	8.876	0	4.994e-6

References

[1] Fuchs, M.; Scheffler, M. Ab initio pseudopotentials for electronic structure calculations of poly-atomic systems using density-functional theory, Comput. Phys. Commun. **1999**, *119*, 67-98.

[2] Zhao, Y. Deng, C.; Tang, D.; Ding, L.; Zhang, Y.; Sheng, H.; Ji, H.; Song, W.; Ma, W.; Chen, C.; Zhao, J. α-Fe_2O_3 as a versatile and efficient oxygen atom transfer catalyst in combination with H2O as the oxygen source, Nature Catal. **2021**, *4*, 684-691.

[3] J. P. Perdew, K. Burke, M. Ernzerhof, Generalized Gradient Approximation Made Simple, Phys. Rev. Lett. **1996**, *77*, 3865-3868.

[4] P. E. Blöchl, Projector augmented-wave method, Phys. Rev. B **1994**, *50*, 17953-17979.

[5] V. I. Anisimov, J. Zaanen, O. K. Andersen, Band theory and Mott insulators: HubbardUinstead of StonerI, Phys. Rev. B **1991**, *44*, 943-954.

[6] V. I Anisimov, F Aryasetiawan, A I Lichtenstein, First-principles calculations of the electronic structure and spectra of strongly correlated systems: the LDA+U method, J. Phys.: Condens. Matter **1997**, *9*, 767-808.

[7] S. Selcuk, A. Selloni, DFT+U Study of the Surface Structure and Stability of Co_3O_4(110): Dependence on U, J. Phys. Chem. C **2015**, *119*, 9973-9979.

[8] S. Kenmoe, D. H. Douma, A. T. Raji, B. M'Passi-Mabiala, T. Götsch, F. Girgsdies, A. Knop-Gericke, R. Schlögl, E. Spohr, X-ray Absorption Near-Edge Structure (XANES) at the O K-Edge of Bulk Co_3O_4: Experimental and Theoretical Studies, Nanomaterials **2022**, *12*, 921.

[9] G. Henkelman, H. Jónsson, Improved tangent estimate in the nudged elastic band method for finding minimum energy paths and saddle points, J. Chem. Phys. **2000**, *113*, 9978.

[10] X. Zhang, J. Liu, B. Zijlstra, I. A. W. Filot, Z. Zhou, S. Sun, E. J. M. Hensen, Optimum Cu nanoparticle catalysts for CO_2 hydrogenation towards methanol, Nano Energy **2018**, *43*, 200-209.

[11] P. Nitoń, A. Żywociński, M. Fiałkowski, R. Hołyst, A "nano-windmill" driven by a flux of water vapour: a comparison to the rotating ATPase, Nanoscale **2013**, *5*, 9732-9738.

[12] Wdowik, U.; Parlinski, K. Lattice dynamics of CoO from first principles. *Phys. Rev. B*, **2007**, *75*, 104306.

[13] Deng, H.; Li, J.; Li, S.; Xia, J.; Walsh, A.; Wei, S. Origin of antiferromagnetism in CoO: A density functional theory study. *Appl. Phys. Lett.*, **2010**, *96*, 162508.

[14] Park, K.; Kolpak, A. Understanding photocatalytic overall water splitting on CoO nanoparticles: Effects of facets, surface stoichiometry, and the CoO/water interface. *J. Catal*., **2018**, *365*, 115-124.